





Continuous operation of large-scale atom arrays in optical lattices

Flavien Gyger ^{1,2} Maximilian Ammenwerth,^{1,2} Renhao Tao ^{1,2,3} Hendrik Timme,^{1,2} Stepan Snigirev ^{1,2,3,4},
Immanuel Bloch,^{1,2,3} and Johannes Zeiher ^{1,2,3,*}

¹Max-Planck-Institut für Quantenoptik, 85748 Garching, Germany

²Munich Center for Quantum Science and Technology (MCQST), 80799 Munich, Germany

³Fakultät für Physik, Ludwig-Maximilians-Universität, 80799 Munich, Germany

⁴PlanQC GmbH, 85748 Garching, Germany



(Received 7 February 2024; accepted 27 June 2024; published 25 July 2024)

Scaling the size of assembled neutral-atom arrays trapped in optical lattices or optical tweezers is an enabling step for a number of applications ranging from quantum simulations to quantum metrology. However, preparation times increase with system size and constitute a severe bottleneck in the bottom-up assembly of large ordered arrays from stochastically loaded optical traps. Here we demonstrate a method to circumvent this bottleneck by recycling atoms from one experimental run to the next, while continuously reloading and adding atoms to the array. Using this approach, we achieve densely packed arrays with more than 1000 atoms stored in an optical lattice, continuously refilled with a 3.5 s cycle time and about 130 atoms reloaded during each cycle. Furthermore, we show that we can continuously maintain such large arrays by simply reloading atoms that are lost from one cycle to the next. Our approach paves the way towards quantum science with large ordered atomic arrays containing thousands of atoms in continuous operation.

DOI: [10.1103/PhysRevResearch.6.033104](https://doi.org/10.1103/PhysRevResearch.6.033104)

I. INTRODUCTION

Atom arrays stored in optical lattices or optical tweezers are a promising platform for quantum simulation, quantum computation, and quantum metrology [1–7]. A usual experimental sequence to control atoms in optical lattices or optical tweezers starts with the preparation of an ensemble, followed by the simulation, calculation, or metrology sequence. Finally, a destructive measurement of the state of the system is performed that typically renders a recycling of atoms from one cycle to the next impossible. The subsequent preparation of a fresh ensemble of atoms requires significantly more time than the actual experimental sequence, leading to a dead time that becomes significantly longer for large arrays. Furthermore, to date, the largest sorted array sizes that have been realized in this way contain a few hundred atoms [7–9]. This naturally calls for a different mode of operation in which only the lost atoms are prepared and replaced in each cycle. While recently demonstrated in a seminal work in bulk gases [10], a reuse of atoms and cyclic operation with microscopic control are challenging and require nondestructive detection in combination with resorting to replenish lost atoms [11,12]. High-fidelity and low-loss detection of single atoms is now

routinely achieved for several species in optical lattice and optical tweezers [13–18]. Although first steps towards extended operation of atom arrays have recently been demonstrated in small-scale systems with finite reservoirs [19,20], truly continuous operation requires schemes for reloading new atoms that do not affect the atomic array already present in the system. Effective strategies to “hide” stored atoms during the reloading of new atoms have recently been demonstrated in dual-element arrays of two alkali-atom species [21,22], where atoms of one species are only minimally affected by forming a magneto-optical trap (MOT) of the other element, thereby enabling continuous operation with arrays of each element prepared in alternation. An alternative route is offered by utilizing the more complex level structure available in alkaline earth(-like) atoms such as strontium or ytterbium. Here two separate optical series with different total spin and metastable states exist, which has proven useful for a variety of applications in combination with microscopic control [20,23–33]. In particular, the metastable states can also be used to effectively hide stored atoms while forming a MOT for the ground-state atoms. Although this level structure has been shown to be well adapted for the preparation of one-dimensional atomic arrays with near-unity filling based on dark-state enhanced loading combined with site control using an acousto-optic deflector (AOD) [32], continuous loading has so far remained an elusive goal.

Here we show a scheme that combines several of the foregoing aspects to realize continuously operated large-scale atom arrays with atom numbers continuously exceeding 1000 atoms and reaching up to 1247 atoms. Our scheme relies on a continuously operated storage zone in an optical lattice, which is periodically replenished from a loading zone and a MOT.

*Contact author: johannes.zeiher@mpq.mpg.de

Published by the American Physical Society under the terms of the [Creative Commons Attribution 4.0 International license](https://creativecommons.org/licenses/by/4.0/). Further distribution of this work must maintain attribution to the author(s) and the published article's title, journal citation, and DOI. Open access publication funded by Max Planck Society.

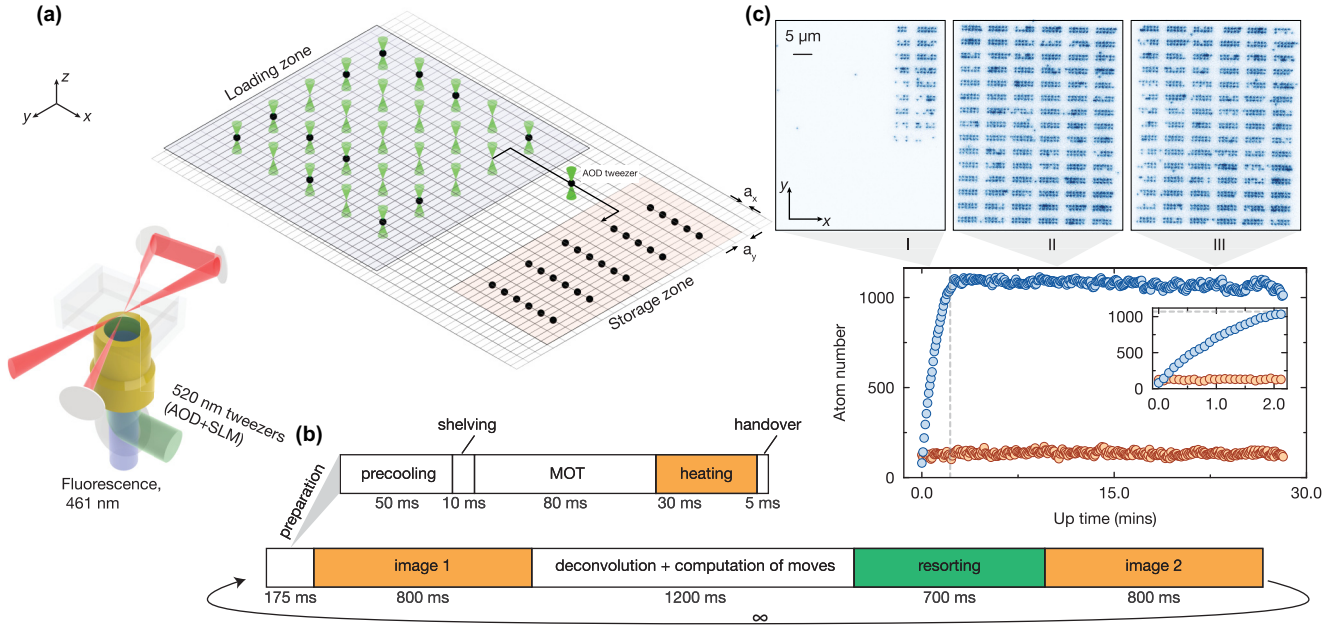


FIG. 1. Concept and demonstration of continuous operation. (a) Main features of our experimental machine. We use a 1040 nm stationary bow-tie optical lattice (red beams) as our physics array (gray grid with $a_x = 579$ nm and $a_y = 1187$ nm). We subdivide the accessible area into a loading zone and a storage zone. The loading zone is overlapped with a stationary tweezer array at 520 nm. Atoms are transported with AODs that steer a single beam in the lattice plane from the loading zone to the storage zone. (b) Experimental sequence of our continuous loading scheme. (c) Exemplary single shots at various instances in time of an iteratively assembled array exceeding 1000 atoms on average. Bottom graph: Atom number of the continuously operated array (blue) and atom number in the loading area (red). Inset: Zoom-in of the atom number in the build-up phase.

Using a bichromatic combination of loading and storage arrays, we achieve excellent spatial control over the loading zone, strongly suppressing loading of sites in the storage register. Loading about 130 new atoms for each cycle, we grow and then continuously maintain an array of atoms in an optical lattice with more than 1000 atoms, which is about eight times larger than the number of atoms loaded during each cycle. Our results mark a paradigm shift in the operation of quantum simulators and quantum computers based on neutral atoms to iteratively assembled and continuously operated arrays.

II. ASSEMBLY OF LARGE ARRAYS

The architecture of our apparatus for continuous operation is shown in Fig. 1 and contains the folded optical lattice at a wavelength of 1040 nm as well as a tweezer array at a wavelength of 520 nm, both described in detail in our previous work [16]. We operate the experiment in one region spanning about $130 \mu\text{m} \times 130 \mu\text{m}$, corresponding to the area that the AODs can currently address. This region is centered above our objective lens and contains about 24 000 trapping sites in a bow-tie lattice. We divide this lattice region into two sub-regions: a loading zone and a storage zone; see Fig. 1(a). The loading zone of the lattice is replenished from a reservoir of 323 tweezers, which are overlapped in three dimensions with the lattice sites. These tweezers are themselves loaded with ^{88}Sr atoms from a dual-stage MOT, on the broad $^1\text{S}_0 - ^1\text{P}_1$ transition at 461 nm and on the narrow-line $^1\text{S}_0 - ^3\text{P}_1$ transition at 689 nm [34]. For high-fidelity detection, we transfer the atoms from the tweezer array into the optical lattice [16,17,27,35] and perform fluorescence imaging therein. Our

cyclic sequence is presented in Fig. 1(b) and has a cycle time of 3.5 s, including data processing.

In the first iteration, we load in average N_L atoms from the MOT into the tweezer array. Then we transfer the atoms in the lattice and perform a high-fidelity and low-loss imaging step [image 1 in Fig. 1(b)] to detect the position of loaded atoms in the loading zone [16]. Detected atoms are subsequently displaced on demand from the loading zone to the storage zone by a moving tweezer controlled by crossed AODs. After resorting, we take an image to benchmark the resorting step. In future implementations, this additional image can be omitted [image 2 in Fig. 1(b)]. Afterwards, we shelve the atoms in the storage zone to the long-lived metastable $^3\text{P}_0$ -state and subsequently refill the tweezer array in the loading zone from a MOT created at the same location overlapped with our lattice. Shelving in the magnetically insensitive clock state protects the stored atoms from loss occurring during the MOT. A subsequent fluorescence image [image 1 in Fig. 1(b)] of both the storage and the loading zone depumps the atoms in $^3\text{P}_0$ back to the ground state $^1\text{S}_0$, revealing unoccupied sites in the storage zone that need to be refilled. The possibility of reusing atoms across experimental runs results in an important scaling advantage for the achievable array sizes. The largest array size is reached when the number of atoms lost during the previous cycle is precisely balanced by the number of atoms replenished in the current cycle. This condition limits the maximally reachable atom number to $N_\infty = \beta N_L$, where the amplification factor

$$\beta = \frac{1 - \alpha_r}{\alpha_c} \quad (1)$$

is proportional to the atom move success probability $1 - \alpha_r$ and inversely proportional to the cycle loss α_c , which quantifies the fraction of stored atoms that are lost from one cycle to the next. The effective number of atoms that can be added to the array in each cycle is $N_{L,\text{eff}} = N_L(1 - \alpha_r)$, which is smaller than the loaded atom number due to atom loss during the transport. In our work, $\alpha_r \approx 30\%$, resulting from atom transport over long distances. For typically achieved cycle losses in this work ($\alpha_c \approx 10\%$), the saturated atom numbers already significantly exceed the number of loaded atoms per cycle N_L ; see Fig. 1(c). We note that, in principle, the loading zone could be fully overlapped with the storage zone by interleaving loading sites and storage sites. Such a configuration would be beneficial, since it increases the available space for the storage area and shortens the move distance between the loading and storage zone. However, in our configuration, the tweezer light at 520 nm induces considerable loss of atoms stored in the 3P_0 states and prevents us from overlapping the two zones. We find evidence that photoionization of the 3P_0 state is responsible for this loss (see Appendix A [29]), which could be mitigated in the future at alternative tweezer wavelengths, such as 813 nm. In the following, we perform a detailed characterization of all steps involved in the continuous operation of our arrays.

III. RELOADING THE RESERVOIR

An important step in the cyclic operation of the array concerns the transfer of atoms from 1S_0 to 3P_0 before reloading the reservoir. Population shelving is currently implemented via a combination of light at 689 nm and 688 nm driving $^1S_0 \rightarrow ^3P_1 \rightarrow ^3S_1$. An additional repumper beam at 707 nm renders the 3P_0 state the only dark state; see Fig. 2(a). The fraction of shelved atoms reaches 97% after 10 ms of pumping, as shown in Fig. 2(c). We note that a higher shelving fraction could be achieved by a combination of coherent shelving and incoherent pumping, which would directly reduce our cycle loss [36]. At our lattice trap depth of 200 μK , the lifetime of atoms in 3P_0 state is 13 s; see Fig. 2(d). The lifetime significantly exceeds the total duration during which the shelved atoms stay in 3P_0 of 115 ms in our sequence, such that holding of shelved atoms by itself induces an insignificant loss. However, we observe a small increase of the shelved atom loss induced by the presence of the MOT, resulting in a total of 6% shelving loss during the 3P_0 preparation and atom reloading steps; see Fig. 2(d) inset. Importantly, we make our MOT without a repumper at 679 nm, which would otherwise deplete the shelved atoms in 3P_0 . This considerably reduces the number of loaded atoms. Still, with optimized parameters, we obtain a filling fraction as high as 40% atom loading probability in the loading tweezer-lattice register sites after parity projection. An additional consequence of the absence of a 3P_0 repumper is the decay of a small fraction of atoms into 3P_0 via $^1D_2 \rightarrow ^3P_2 \rightarrow ^3S_1$, where they become indistinguishable from the shelved atoms in the stored array. To counteract this effect, the 1D_2 state could be repumped to higher-lying 1P_1 -states on transitions either at 716 nm or 448 nm [37], which would increase the MOT loading fraction and remove defects originating from accidentally shelved atoms in 3P_0 during the MOT stage.

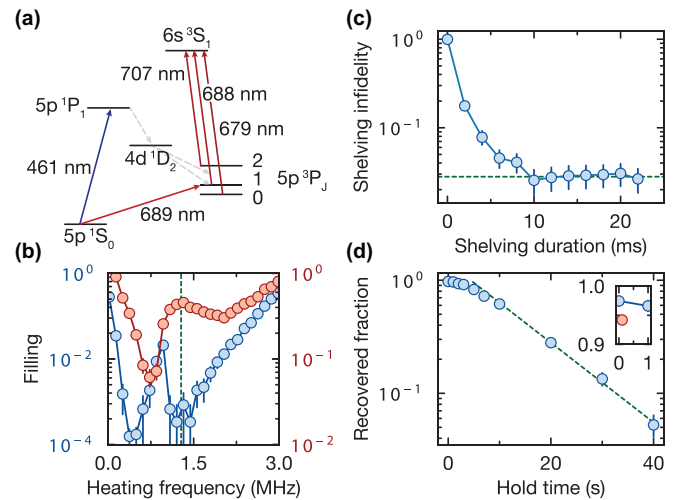


FIG. 2. Shelving and trap-selective heating. (a) Energy level of ^{88}Sr . (b) Resulting filling after a trap-selective 689 nm Sisyphus-heating pulse applied to atoms trapped in the lattice (blue) and in the combined tweezer-lattice potential (red) as a function of the applied frequency detuning. The trace is normalized to the loading fraction without heating pulse for the lattice and normalized to our tweezer number (323) for the combined potential. An extinction of 5×10^{-4} for ground-state lattice atoms is achieved when choosing a frequency detuning of 1.28 MHz (green dashed line), while the atoms in the combined tweezer-lattice potential remain almost unaffected with a loading fraction of 40%. (c) Round-trip shelving infidelity as a function of shelving duration, reaching 3% (green dashed line) after 10 ms. (d) Shelving lifetime in our lattice at 200 μK , reaching 13 s, extracted from an exponential fit to the last four data points (green dashed line). Inset: Zoom-in of the hold time region below one second. The red dot indicates our actual recovered fraction when a MOT is created within the hold time.

Importantly, the MOT loads the entire lattice, including the loading zone and the storage zone. To remove ground-state atoms from the lattice everywhere except from the sites overlapped with the tweezer array in the loading zone, we subsequently apply an essential trap-selective heating pulse. This heating pulse is optimized to remove ground-state atoms in the lattice, while leaving both ground-state atoms in the tweezer array and 3P_0 atoms in the lattice intact; see Fig. 2(b). We do not observe any additional loss of shelved atoms resulting from our heating pulse within error bars of our measurement. The red data point in Fig. 2(d) inset includes the combined effect of the MOT overlapping with the storage array and the heating pulse on the stored atoms in 3P_0 , and shows only a slight reduction of $\approx 3\%$ for both effects combined, which we mostly attribute to the overlapping MOT. To realize this selective removal of atoms, we use a beam at 689 nm tuned to a repulsive Sisyphus heating regime. This heating feature is unique to transitions narrow enough to spatially resolve the differential trap depth between the 1S_0 state and the 3P_1 state. For the chosen detuning, a net kinetic energy gain is realized between subsequent excitation-decay cycles, and thus leads to a fast, highly parallel, and well-controllable heating mechanism of ground-state atoms in the lattice. The atoms in the loading zone experience an additional light shift from the combined bichromatic lattice-tweezer

potential which shields them from the heating resonance, and thus they remain trapped; see Fig. 2(b). Consequently, our selective heating pulse effectively removes all atoms in 1S_0 that experience only the lattice potential with an extinction of more than 5×10^{-4} . This prevents uncontrolled storage of atoms directly loaded from the MOT in the storage zone. The heating pulse is performed using a trap depth of 200 μK and 430 μK for the lattice and the tweezers, respectively, and using an intensity of 40 mW/cm^2 for the heating beam. Alternatively, site-selective parallel addressing can also be used to hide already loaded sites from being further loaded, as effectively shown in one dimension [32], with direct extensions using state-selective parallel addressing in higher dimensions [38].

IV. RESORTING IN AN OPTICAL LATTICE

The next important step in our cyclic sequence is the rearrangement of newly loaded atoms to vacancies in the target of the sorted array. We perform such moves using a pair of AODs similar to previous work [9,17,31,39]. In contrast to the case of optical tweezer arrays, atoms moving through lattice sites experience a large periodic trap depth modulation, potentially leading to strong heating. In the special case of a bow-tie lattice, this modulation can be strongly reduced by moving atoms in between the lattice sites, thereby ameliorating any heating effects; see Fig. 3(a). In line with this expectation, we directly observe that long moves in between the lattice sites exhibit a significantly higher success probability than moves through lattice sites; see Fig. 3(d). In this measurement and during the continuous loading operation, all moves are performed with a peak velocity of 54 $\mu\text{m}/\text{ms}$. In particular, for the long moves considered in this work, movement between sites is crucial. Our lattice has spacings between sites of $a_x = 579 \text{ nm}$ and $a_y = 1187 \text{ nm}$ along the x and y axis, respectively, and is therefore particularly suited for horizontal moves; see Fig. 3(a). To optimally leverage the favorable geometry of our lattice, our resorting procedure has been designed to predominantly move between lattice sites with a five-stroke move pattern; see Fig. 3(b). The first stroke removes the atom out of its lattice site and brings it between lattice sites. The second stroke displaces the atom outside of the loading area. The third and fourth strokes adjust the vertical (y axis) and horizontal (x axis) positions, respectively, to almost match that of its final destination, and finally the last stroke inserts the atom in its final location; see Fig. 3(b). Each move consists of (1) a slow ramp-up of the moving tweezer potential depth to about ten times the lattice depth to extract the target atom out of the lattice, (2) a sequence of parameterized frequency chirps encoding velocity profiles and turns, and (3) a final ramp-down of the tweezer depth to release the atom in the desired target lattice site in the storage zone. The initial and final intensity ramp durations are 400 μs each, to ensure adiabaticity [40]. No cooling is present during the entire resorting operation.

The imperfect resorting process affects continuous loading in two ways: First, it reduces the effective atom number $N_{L,\text{eff}}$ that can be maximally added to the storage array in each cycle when atoms are lost during transfer. Second, by traveling at a close distance to an already stored atom,

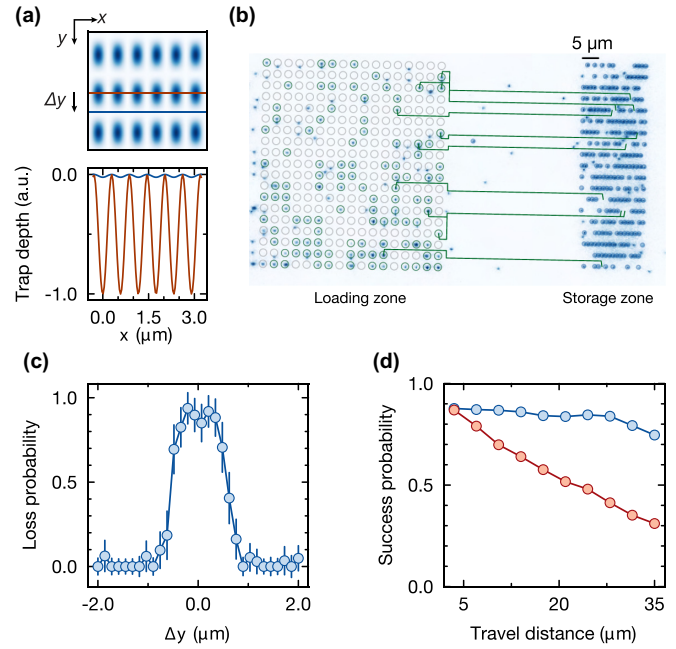


FIG. 3. Atom rearrangement. (a) Upper graph: Energy landscape of our folded lattice. Lower graph: Reduction of the trap depth modulation experienced by an atom traveling between the lattice sites (blue line in the upper graph), as compared to through the lattice sites (red line in the upper graph). (b) Resorting algorithm favoring horizontal moves along corridors between the lattice sites. (c) Atom loss probability as a function of the distance between an occupied lattice site and the traveling resorting tweezer. Disturbance leading to atom loss are observed below 1 μm of distance. (d) Atom move success probability $1 - \alpha_r$ as a function of the traveling distance, when the moves are performed through the lattice sites (red points) and when they are performed between the lattice sites (blue points). The atom move success probability is defined as the probability of not losing the atom during the entire move operation.

the unintended perturbation of the trapping site can result in a loss of the stored atom and thus directly increases the cycle loss. We observe a corresponding limit for the minimum distance between a stored atom and the trajectory of the moving tweezer, which is approximately equal to 1 μm ; see Fig. 3(c). This minimum distance sets a limit for the minimal achievable spacing between atoms in the storage register. The total resorting duration for each cycle is about 700 ms. This duration could be drastically reduced by implementing a more complex parallel resorting scheme [11,17,41,42].

V. CONTINUOUS OPERATION

Finally, combining all steps, we demonstrate the ability to build and maintain a large-scale, densely packed tweezer array for more than an hour; see Fig. 4. After the initial loading stage, the number of atoms stored in the array remained above 1000 atoms for most of the operation time. From the atom loss within and across different cycles, we can extract both the cycle loss α_c , as well as the resorting loss α_r that enter in a simple model for the build-up and saturation of the stored

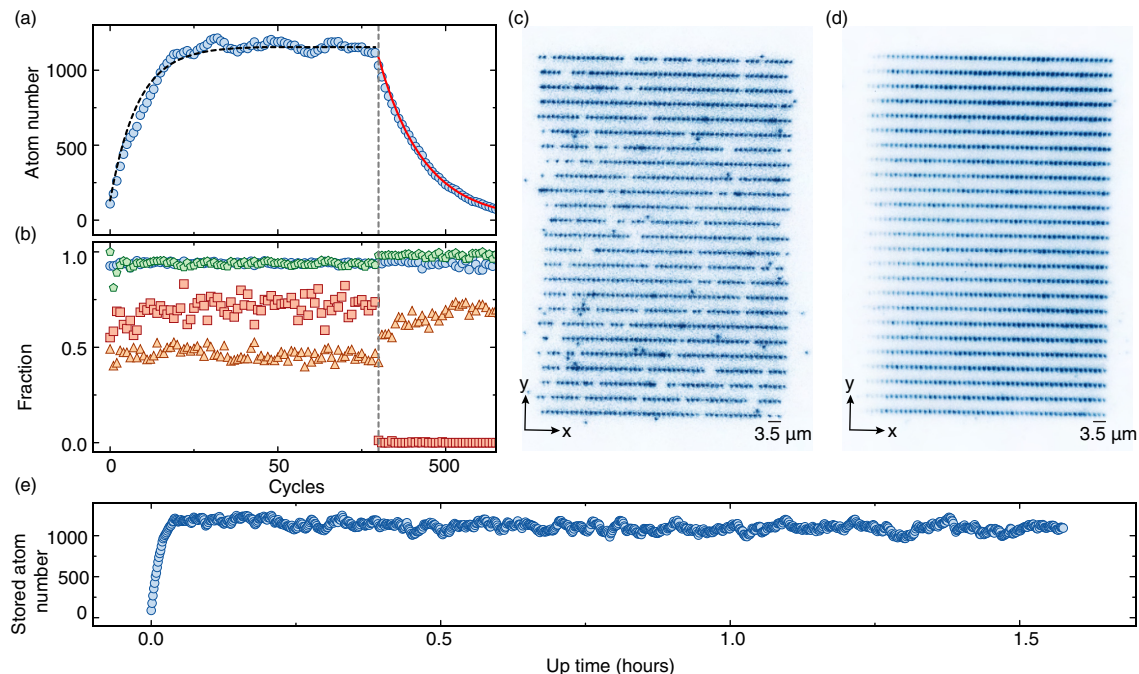


FIG. 4. Characterization of continuous operation. (a) Number of atoms in the storage area as a function of cycles. After 80 cycles, we disable the resorting and let the array naturally decay. The black dashed line is our model from Eqs. (2) with measured average parameters, while the red line is an exponential fit that enables us to measure the cycle loss α_c (neglecting the influence of resorting in this case). (b) Evolution of the loading fraction (orange triangles), resorting move success probability (red squares), shelved survival fraction (blue circles), and stored survival fraction during resorting (green pentagons) as a function of cycles. (c) Single-shot image of the storage array containing 1230 atoms. (d) Average image of the storage array. (e) Continuous operation of the array for more than 1.5 h.

atom number N_i at each cycle i ,

$$N_{i+1} = (1 - \alpha_c)N_i + (1 - \alpha_r) \cdot N_L, \quad i = 0, 1, \dots,$$

$$N_\infty = \frac{(1 - \alpha_r)N_L}{\alpha_c}. \quad (2)$$

The dashed line in Fig. 4(a) is computed from these equations using time-average values of the measured cycle loss and resorting loss, and is in excellent agreement with the measured atom number. Four parameters of interest are extracted from the occupation matrices and plotted in Fig. 4(b): (1) the loading fraction, defined as the number of loaded atoms in the loading zone N_L normalized to total number of tweezer sites (323); (2) the resorting move success probability $1 - \alpha_r$, defined as the number of loaded atoms that are successfully moved into the storage zone, normalized to the total loaded atom number N_L ; (3) the shelved survival fraction, defined as the number of atoms that survive the shelving, holding and repumping operation between two cycles, normalized to the total atom number in the storage zone; and (4) the stored atom survival fraction during resorting, defined as the number of atoms in the stored array that survive the resorting procedure without being moved themselves, normalized to the total atom number in the storage zone. We observe that, in our system, both the shelved survival fraction and the stored atom survival fraction during resorting contribute equally to the cycle loss. After 80 cycles, we disable the resorting operation and let the stored array decay. Subsequently, we observe that (1) the loading curve rises, since the loaded atoms are no longer removed and accumulate in the loading zone and (2) the

stored atoms survival fraction during resorting rises, since no resorting operation disturbs the stored array.

In order to investigate the observed fluctuations on top of the steady-state atom number, a detailed correlation analysis relating the measured final atom numbers to the extracted cycle loss, the resorting infidelity, and the reloaded atom number directly reveals that the fluctuations of the final atom number are most strongly correlated with the cycle loss; see Appendix B. Such a behavior is expected from the inverse scaling of steady-state atom number with cycle loss and highlights the large potential gains in a further optimized sequence.

VI. CONCLUSION AND OUTLOOK

To conclude, we have presented a first realization of densely packed, continuously loaded atom arrays stored in an optical lattice. Prospectively, we expect that our technique could allow for the assembly of significantly larger atom arrays than what we have demonstrated. One improvement of our experiment would be to move the position of the MOT slightly away from the storage array. This would mitigate the need to empty the storage array from accidentally loaded atoms, enable parallel MOT and the storage array operation, and reduce the small effect of unwanted off-resonant scattering from MOT light on the storage atoms further. In previous work, the efficiency of shelving atoms in 3P_0 has been shown to reach 99.7% [36]. For a clock-state lifetime of the order of 100 s with a reduced lattice potential [43] and a typical MOT stage of 100 ms duration, the shelved atoms loss during the MOT stage could be reduced to 0.1%, leading to a total

shelving loss as low as 0.4%. Assuming our measured vacuum lifetime of 273 s, the typical vacuum-limited loss for a 1-s cycle time experiment is roughly also equal to 0.4%, leading to a total cycle loss of about $\alpha_c \approx 0.8\%$. Together with an atom loss due to resorting moves α_r that could be reduced to $\approx 2\%$ [17], Eq. (1) predicts the achievable amplification factor to reach $\beta > 100$. With such a large amplification, one could reach about 10 000 atoms in a single array with 100 loaded atoms at each cycle, provided that a sufficient area for storage and high-fidelity detection is available [16]. Deterministically loaded arrays [24,44] or directly loaded lattices [16] as loading zones could further boost the achievable steady-state atom numbers potentially by orders of magnitude. We want to emphasize that, compared to directly assembling such a large number of atoms in a single experimental cycle, continuous loading has the benefit of moving only the newly loaded atoms for each cycle, thus reducing both move-induced losses as well as the resorting time overhead by the amplification factor β . We foresee our large-scale continuously operated arrays to find applications in quantum simulation, quantum optics, and quantum metrology. For example, we anticipate that continuously loaded arrays can be utilized as light-matter interfaces based on subwavelength ordering [45,46], where lost atoms can be continuously replenished from the loading area. For quantum metrology, in particular optical clocks, our large arrays enter an interesting regime of large-scale but still microscopically addressable systems that bridge the gap between smaller [23], potentially quantum-enhanced [31] ensembles and large-scale, highly precise classical ensembles without microscopic control [47]. Moreover, maintaining coherence during the reloading stage, for example, for atoms placed in a specially shielded physics array, would open up exciting perspectives for both quantum metrology or quantum information tasks [20,22]. We foresee the possibility to use qubit encodings in the metastable manifold, such as the recently demonstrated fine-structure qubit encoding in strontium [48,49], in combination with dynamical decoupling similar to recently demonstrated dual-element realizations [22], motional qubit encodings [50], or nuclear-spin qubit encodings in $^3\text{P}_0$ as recently realized in ytterbium [28,29]. Such large, continuously maintained atom arrays combined with the recently demonstrated fast, high-fidelity quantum gates [51] and elementary logical quantum circuits [9] make neutral atoms a promising platform for quantum computing and quantum simulation at scale.

Note added. We recently became aware of related work, where similar results have been reported using arrays of ^{171}Yb [52].

ACKNOWLEDGMENTS

We acknowledge funding by the Max Planck Society (MPG) the Deutsche Forschungsgemeinschaft (DFG, German Research Foundation) under Germany's Excellence Strategy—EXC-2111—390814868, from the Munich Quantum Valley initiative as part of the High-Tech Agenda Plus of the Bavarian State Government, and from the BMBF through the programs MUNIQ-Atoms and MAQCS. This publication has also received funding under Horizon Europe program HORIZON-CL4-2022-QUANTUM-02-SGA via Project No. 101113690

(PASQuanS2.1). J.Z. acknowledges support from the BMBF through the program Quantum technologies—from basic research to market (SNAQC, Grant No. 13N16265). M.A. and R.T. acknowledge funding from the International Max Planck Research School (IMPRS) for Quantum Science and Technology. M.A. acknowledges support through a fellowship from the Hector Fellow Academy. F.G. acknowledges funding from the Swiss National Fonds (Fund No. P500PT_203162).

APPENDIX A: $^3\text{P}_0$ IONIZATION IN 520 nm TWEEZERS

In our experiments we find the $^3\text{P}_0$ lifetime of atoms in 520 nm tweezers to be limited to 40 ms for tweezers at a trap depth of 300 μK , and to depend quadratically on the trap depth, as shown in Fig. 5. This suggests that light at 520 nm could ionize atoms stored in $^3\text{P}_0$ in a two-photon excitation. In our continuous loading experiment, we observed that the shelving lifetime was considerably decreased for atoms in the loading zone, even when atoms were trapped in a lattice site not overlapping with a tweezer. As a consequence of this observation, we spatially separated our loading and storage zone to mitigate this extra tweezer-induced cycle loss. We anticipate that using another wavelength for the tweezers (e.g., 813 nm) would sidestep this issue and increase the available space for both the loading and storage zones.

APPENDIX B: CORRELATION ANALYSIS ON THE ATOM NUMBER FLUCTUATION IN THE STORED ARRAY

To understand the origin of the atom number fluctuation in continuous operation of the stored array, we study the correlations between the fluctuations and a set of parameters based on the atom occupation during various stages of the sequence. In this analysis, we consider only atoms placed at sites of the stored array defined by a custom target; all atoms which are not in a site of the stored array, even if they are placed in the storage zone (defects), are ignored. We define the survival fraction s_{mn} as the sum over all stored array sites that are filled in both image m and image n , normalized to the occupation of image m . Therefore, $0 \leq s_{mn} \leq 1$ quantifies the atoms in the stored array that survived from image m to a succeeding image n . Similarly, we define the gain fraction a_{mn} as the sum over

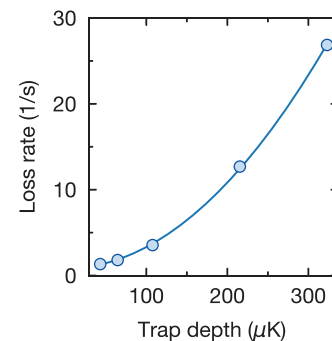


FIG. 5. $^3\text{P}_0$ ionization from 520 nm tweezers. Measured and parabolic fit of $^3\text{P}_0$ lifetime as a function of the tweezers trap depth. The extracted quadratic contribution to the loss rate is $250 \text{ s}^{-1} (\text{mK})^{-2}$.

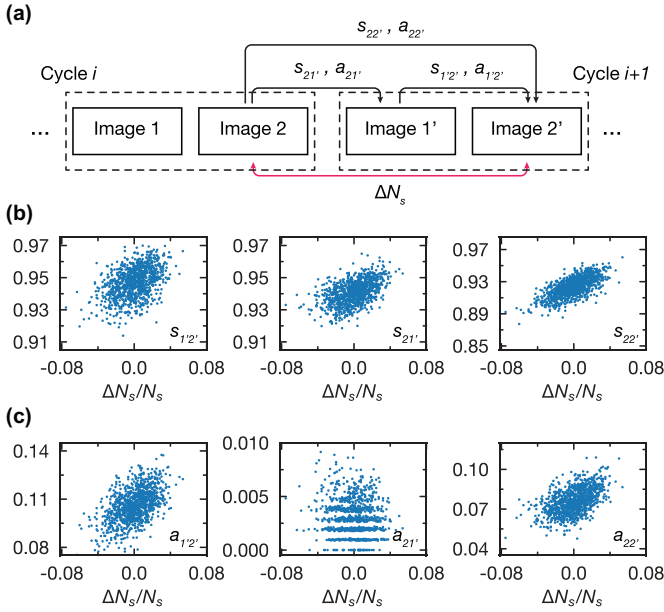


FIG. 6. Correlations analysis on atom number fluctuation. (a) Sequence of images taken during continuous loading for the current cycle i and the next cycle $i + 1$ indicating between which images various quantities of interest are computed at the cycle i ; see text for more details. (b) Survival fraction of atoms from one image to another, as a function of atom number fluctuation. (c) Gain fraction of atoms from one image to another, as a function of atom number fluctuation.

all stored array sites that are empty in image m but filled in image n , normalized to the occupation of image n . Therefore, $0 \leq a_{mn} \leq 1$ quantifies the atoms that have appeared in the stored array from image m to a succeeding image n . For the survival fraction s_{mn} and gain fraction a_{mn} , we label the

TABLE I. Pearson coefficients of the correlated quantities.

Quantity	$s_{1'2'}$	$s_{21'}$	$s_{22'}$	$a_{1'2'}$	$a_{21'}$	$a_{22'}$
Pearson coefficient	0.46	0.50	0.68	0.53	-0.12	0.51

images using an augmented image index $m, n = \{1, 2, 1', 2'\}$, where the indices 1 and 2 refer, respectively, to the first and second image of a cycle i , and where the indices 1' and 2' refer, respectively, to the first and second image of the next cycle $i + 1$; see Fig. 6(a). The fluctuations are quantified by the quantity $\Delta N_s/N_s$, where N_s is the number of filled sites in our stored array, while ΔN_s is defined as the difference of the number of filled sites in the stored array between two consecutive cycles. The correlations of the atom number fluctuations $\Delta N_s/N_s$ with s_{mn} and a_{mn} are summarized in Figs. 6(b) and 6(c). We quantify the strength of the correlations using the Pearson coefficient $\rho(X, Y)$ between two random variables X and Y , defined as

$$\rho(X, Y) = \frac{\text{cov}(X, Y)}{\sigma(X)\sigma(Y)}, \quad (\text{B1})$$

where cov is the covariance and $\sigma(X)$, $\sigma(Y)$ are the standard deviations of X and Y , respectively. We observe that $\Delta N_s/N_s$ correlates most strongly with the cycle survival ($s_{22'}$), comprising the contribution of the shelved survival fraction ($s_{21'}$) and the stored atom survival fraction ($s_{1'2'}$); see Table I.

Interestingly, we also observe a nonvanishing value of $a_{21'}$, despite no atoms being intentionally added to the array between the second image of the cycle i and the first image of the cycle $i + 1$. Since neither imperfect heating nor atoms accidentally shelved in 3P_0 during the MOT yield large enough contributions to explain the observed increased atom number from one cycle to the next, we speculate this effect to mostly arise from misclassification of our deconvolution algorithm.

- [1] M. Saffman, Quantum computing with atomic qubits and Rydberg interactions: Progress and challenges, *J. Phys. B: At. Mol. Opt. Phys.* **49**, 202001 (2016).
- [2] A. Browaeys and T. Lahaye, Many-body physics with individually controlled Rydberg atoms, *Nat. Phys.* **16**, 132 (2020).
- [3] A. M. Kaufman and K.-K. Ni, Quantum science with optical tweezer arrays of ultracold atoms and molecules, *Nat. Phys.* **17**, 1324 (2021).
- [4] A. J. Daley, I. Bloch, C. Kokail, S. Flannigan, N. Pearson, M. Troyer, and P. Zoller, Practical quantum advantage in quantum simulation, *Nature (London)* **607**, 667 (2022).
- [5] M. Morgado and S. Whitlock, Quantum simulation and computing with Rydberg-interacting qubits, *AVS Quantum Sci.* **3**, 023501 (2021).
- [6] H. Katori, Optical lattice clocks and quantum metrology, *Nat. Photonics* **5**, 203 (2011).
- [7] L. Pause, L. Sturm, M. Mittenbühler, S. Amann, T. Preuschoff, D. Schäffner, M. Schlosser, and G. Birkel, Supercharged two-dimensional tweezer array with more than 1000 atomic qubits, *Optica* **11**, 222 (2024).
- [8] K.-N. Schymik, B. Ximenez, E. Bloch, D. Dreon, A. Signoles, F. Nogrette, D. Barredo, A. Browaeys, and T. Lahaye, *In situ* equalization of single-atom loading in large-scale optical tweezer arrays, *Phys. Rev. A* **106**, 022611 (2022).
- [9] D. Bluvstein, S. J. Evered, A. A. Geim, S. H. Li, H. Zhou, T. Manovitz, S. Ebadi, M. Cain, M. Kalinowski, D. Hangleiter *et al.*, Logical quantum processor based on reconfigurable atom arrays, *Nature (London)* **626**, 58 (2024).
- [10] C.-C. Chen, R. González Escudero, J. Minář, B. Pasquiou, S. Bennetts, and F. Schreck, Continuous Bose-Einstein condensation, *Nature (London)* **606**, 683 (2022).
- [11] M. Endres, H. Bernien, A. Keesling, H. Levine, E. R. Anschuetz, A. Krajenbrink, C. Senko, V. Vuletic, M. Greiner, and M. D. Lukin, Atom-by-atom assembly of defect-free one-dimensional cold atom arrays, *Science* **354**, 1024 (2016).
- [12] D. Barredo, S. de Léséleuc, V. Lienhard, T. Lahaye, and A. Browaeys, An atom-by-atom assembler of defect-free arbitrary two-dimensional atomic arrays, *Science* **354**, 1021 (2016).
- [13] C. Gross and I. Bloch, Quantum simulations with ultracold atoms in optical lattices, *Science* **357**, 995 (2017).
- [14] J. P. Covey, I. S. Madjarov, A. Cooper, and M. Endres, 2000-times repeated imaging of strontium atoms in clock-magic tweezer arrays, *Phys. Rev. Lett.* **122**, 173201 (2019).

- [15] S. Sashkin, J. T. Wilson, B. Grinkemeyer, and J. D. Thompson, Narrow-line cooling and imaging of ytterbium atoms in an optical tweezer array, *Phys. Rev. Lett.* **122**, 143002 (2019).
- [16] R. Tao, M. Ammenwerth, F. Gyger, I. Bloch, and J. Zeiher, High-fidelity detection of large-scale atom arrays in an optical lattice, *Phys. Rev. Lett.* **133**, 013401 (2024).
- [17] A. W. Young, S. Geller, W. J. Eckner, N. Schine, S. Glancy, E. Knill, and A. M. Kaufman, An atomic boson sampler, *Nature* **629**, 311 (2023).
- [18] K. N. Blodgett, D. Peana, S. S. Phatak, L. M. Terry, M. P. Montes, and J. D. Hood, Imaging a ${}^6\text{Li}$ atom in an optical tweezer 2000 times with λ -enhanced gray molasses, *Phys. Rev. Lett.* **131**, 083001 (2023).
- [19] L. Pause, T. Preuschoff, D. Schäffner, M. Schlosser, and G. Birkel, Reservoir-based deterministic loading of single-atom tweezer arrays, *Phys. Rev. Res.* **5**, L032009 (2023).
- [20] M. A. Norcia, W. Cairncross, K. Barnes, P. Battaglino, A. Brown, M. Brown, K. Cassella, C.-A. Chen, R. Coxe, D. Crow *et al.*, Midcircuit qubit measurement and rearrangement in a ${}^{171}\text{Yb}$ atomic array, *Phys. Rev. X* **13**, 041034 (2023).
- [21] K. Singh, S. Anand, A. Pocklington, J. T. Kemp, and H. Bernien, Dual-element, two-dimensional atom array with continuous-mode operation, *Phys. Rev. X* **12**, 011040 (2022).
- [22] K. Singh, C. E. Bradley, S. Anand, V. Ramesh, R. White, and H. Bernien, Mid-circuit correction of correlated phase errors using an array of spectator qubits, *Science* **380**, 1265 (2023).
- [23] A. W. Young, W. J. Eckner, W. R. Milner, D. Kedar, M. A. Norcia, E. Oelker, N. Schine, J. Ye, and A. M. Kaufman, Half-minute-scale atomic coherence and high relative stability in a tweezer clock, *Nature (London)* **588**, 408 (2020).
- [24] A. Jenkins, J. W. Lis, A. Senoo, W. F. McGrew, and A. M. Kaufman, Ytterbium nuclear-spin qubits in an optical tweezer array, *Phys. Rev. X* **12**, 021027 (2022).
- [25] S. Ma, A. P. Burgers, G. Liu, J. Wilson, B. Zhang, and J. D. Thompson, Universal gate operations on nuclear spin qubits in an optical tweezer array of ${}^{171}\text{Yb}$ atoms, *Phys. Rev. X* **12**, 021028 (2022).
- [26] A. Urech, I. H. A. Knottnerus, R. J. C. Spreeuw, and F. Schreck, Narrow-line imaging of single strontium atoms in shallow optical tweezers, *Phys. Rev. Res.* **4**, 023245 (2022).
- [27] N. Schine, A. W. Young, W. J. Eckner, M. J. Martin, and A. M. Kaufman, Long-lived Bell states in an array of optical clock qubits, *Nat. Phys.* **18**, 1067 (2022).
- [28] J. W. Lis, A. Senoo, W. F. McGrew, F. Rönchen, A. Jenkins, and A. M. Kaufman, Midcircuit operations using the OMG architecture in neutral atom arrays, *Phys. Rev. X* **13**, 041035 (2023).
- [29] S. Ma, G. Liu, P. Peng, B. Zhang, S. Jandura, J. Claes, A. P. Burgers, G. Pupillo, S. Puri, and J. D. Thompson, High-fidelity gates and mid-circuit erasure conversion in an atomic qubit, *Nature (London)* **622**, 279 (2023).
- [30] P. Scholl, A. L. Shaw, R. B.-S. Tsai, R. Finkelstein, J. Choi, and M. Endres, Erasure conversion in a high-fidelity Rydberg quantum simulator, *Nature (London)* **622**, 273 (2023).
- [31] W. J. Eckner, N. Darkwah Oppong, A. Cao, A. W. Young, W. R. Milner, J. M. Robinson, J. Ye, and A. M. Kaufman, Realizing spin squeezing with Rydberg interactions in an optical clock, *Nature (London)* **621**, 734 (2023).
- [32] A. L. Shaw, P. Scholl, R. Finkelstein, I. S. Madjarov, B. Grinkemeyer, and M. Endres, Dark-state enhanced loading of an optical tweezer array, *Phys. Rev. Lett.* **130**, 193402 (2023).
- [33] A. L. Shaw, R. Finkelstein, R. B.-S. Tsai, P. Scholl, T. H. Yoon, J. Choi, and M. Endres, Multi-ensemble metrology by programming local rotations with atom movements, *Nat. Phys.* **20**, 195 (2024).
- [34] X. Xu, T. H. Loftus, J. L. Hall, A. Gallagher, and J. Ye, Cooling and trapping of atomic strontium, *J. Opt. Soc. Am. B* **20**, 968 (2003).
- [35] A. W. Young, W. J. Eckner, N. Schine, A. M. Childs, and A. M. Kaufman, Tweezer-programmable 2D quantum walks in a Hubbard-regime lattice, *Science* **377**, 885 (2022).
- [36] I. S. Madjarov, J. P. Covey, A. L. Shaw, J. Choi, A. Kale, A. Cooper, H. Pichler, V. Schkolnik, J. R. Williams, and M. Endres, High-fidelity entanglement and detection of alkaline-earth Rydberg atoms, *Nat. Phys.* **16**, 857 (2020).
- [37] J. Samland, S. Bennetts, C.-C. Chen, R. G. Escudero, F. Schreck, and B. Pasquiou, Optical pumping of $5s4d^1D_2$ strontium atoms for laser cooling and imaging, *Phys. Rev. Res.* **6**, 013319 (2024).
- [38] B. Zhang, P. Peng, A. Paul, and J. D. Thompson, Scaled local gate controller for optically addressed qubits, *Optica* **11**, 227 (2024).
- [39] D. Ohl de Mello, D. Schäffner, J. Werkmann, T. Preuschoff, L. Kohfahl, M. Schlosser, and G. Birkel, Defect-free assembly of 2D clusters of more than 100 single-atom quantum systems, *Phys. Rev. Lett.* **122**, 203601 (2019).
- [40] C. Weitenberg, S. Kuhr, K. Mølmer, and J. F. Sherson, Quantum computation architecture using optical tweezers, *Phys. Rev. A* **84**, 032322 (2011).
- [41] S. Ebadi, T. T. Wang, H. Levine, A. Keesling, G. Semeghini, A. Omran, D. Bluvstein, R. Samajdar, H. Pichler, W. W. Ho *et al.*, Quantum phases of matter on a 256-atom programmable quantum simulator, *Nature (London)* **595**, 227 (2021).
- [42] W. Tian, W. J. Wee, A. Qu, B. J. M. Lim, P. R. Datla, V. P. W. Koh, and H. Loh, Parallel assembly of arbitrary defect-free atom arrays with a multitweezer algorithm, *Phys. Rev. Appl.* **19**, 034048 (2023).
- [43] S. Dörscher, R. Schwarz, A. Al-Masoudi, S. Falke, U. Sterr, and C. Lisdat, Lattice-induced photon scattering in an optical lattice clock, *Phys. Rev. A* **97**, 063419 (2018).
- [44] M. O. Brown, T. Thiele, C. Kiehl, T.-W. Hsu, and C. A. Regal, Gray-molasses optical-tweezer loading: Controlling collisions for scaling atom-array assembly, *Phys. Rev. X* **9**, 011057 (2019).
- [45] J. Rui, D. Wei, A. Rubio-Abadal, S. Hollerith, J. Zeiher, D. M. Stamper-Kurn, C. Gross, and I. Bloch, A subradiant optical mirror formed by a single structured atomic layer, *Nature (London)* **583**, 369 (2020).
- [46] S. J. Masson, J. P. Covey, S. Will, and A. Asenjo-Garcia, Dicke superradiance in ordered arrays of multilevel atoms, *PRX Quantum* **5**, 010344 (2024).
- [47] T. Bothwell, C. J. Kennedy, A. Aeppli, D. Kedar, J. M. Robinson, E. Oelker, A. Staron, and J. Ye, Resolving the gravitational redshift across a millimetre-scale atomic sample, *Nature (London)* **602**, 420 (2022).
- [48] S. Pucher, V. Klüsener, F. Spriestersbach, J. Geiger, A. Schindewolf, I. Bloch, and S. Blatt, Fine-structure qubit encoded in metastable strontium trapped in an optical lattice, *Phys. Rev. Lett.* **132**, 150605 (2024).

- [49] G. Unnikrishnan, P. Ilzhöfer, A. Scholz, C. Hölzl, A. Götzelmann, R. K. Gupta, J. Zhao, J. Krauter, S. Weber, N. Makki *et al.*, Coherent control of the fine-structure qubit in a single alkaline-earth atom, *Phys. Rev. Lett.* **132**, 150606 (2024).
- [50] P. Scholl, A. L. Shaw, R. Finkelstein, R. B.-S. Tsai, J. Choi, and M. Endres, Erasure-cooling, control, and hyper-entanglement of motion in optical tweezers, [arXiv:2311.15580](https://arxiv.org/abs/2311.15580).
- [51] S. J. Evered, D. Bluvstein, M. Kalinowski, S. Ebadi, T. Manovitz, H. Zhou, S. H. Li, A. A. Geim, T. T. Wang, N. Maskara *et al.*, High-fidelity parallel entangling gates on a neutral-atom quantum computer, *Nature (London)* **622**, 268 (2023).
- [52] M. Norcia, H. Kim, W. Cairncross, M. Stone, A. Ryou, M. Jaffe, M. Brown, K. Barnes, P. Battaglino, A. Brown *et al.*, Iterative assembly of ^{171}Yb atom arrays in cavity-enhanced optical lattices, [arXiv:2401.16177](https://arxiv.org/abs/2401.16177).